Cite as: J. Liu *et al.*, *Science* 10.1126/science.aay6018 (2020).

N^6-methyladenosine of chromosome-associated regulatory RNA regulates chromatin state and transcription

Jun Liu[1,2]*, Xiaoyang Dou[1,2]*, Chuanyuan Chen[3,4,5,6]*, Chuan Chen[7], Chang Liu[1,2], Meng Michelle Xu[8], Siqi Zhao[3,4,5], Bin Shen[9], Yawei Gao[7]†, Dali Han[3,4,5,6]†, Chuan He[1,2,10]†

[1]Department of Chemistry and Institute for Biophysical Dynamics, The University of Chicago, Chicago, IL 60637, USA. [2]Howard Hughes Medical Institute, Chicago, IL 60637, USA. [3]Key Laboratory of Genomic and Precision Medicine, Beijing Institute of Genomics, Chinese Academy of Sciences, Beijing 100101, China. [4]National Center for Bioinformation, Beijing 100101, China. [5]Institute for Stem Cell and Regeneration, Chinese Academy of Sciences, Beijing 100101, China. [6]College of Future Technology, Sino-Danish College, University of Chinese Academy of Sciences, Beijing 100049, China. [7]Institute for Regenerative Medicine, Shanghai East Hospital, Shanghai Key Laboratory of Signaling and Disease Research, Frontier Science Center for Stem Cell Research, School of Life Sciences and Technology, Tongji University, Shanghai 200120, China. [8]Department of Basic Medical Sciences, School of Medicine, Institute for Immunology, Beijing Key Lab for Immunological Research on Chronic Diseases, THU-PKU Center for Life Sciences, Tsinghua University, Beijing 100084. China. [9]State Key Laboratory of Reproductive Medicine, Department of Histology and Embryology, Nanjing Medical University, Nanjing 211166, China. [10]Department of Biochemistry and Molecular Biology, The University of Chicago, Chicago, IL 60637, USA.

*These authors contributed equally to this work.

†Corresponding author. Email: chuanhe@uchicago.edu (C.H.); handl@big.ac.cn (D.H.); gaoyawei@tongji.edu.cn (Y.G.)

N^6-methyladenosine (m^6A) regulates stability and translation of messenger RNA (mRNA) in various biological processes. Here, we showed that knockout of the m^6A writer *Mettl3* or a nuclear reader *Ythdc1* in mouse embryonic stem cells increases chromatin accessibility and activates transcription in an m^6A-dependent manner. We found that METTL3 deposits m^6A modifications on chromosome-associated regulatory RNAs (carRNAs), including promoter-associated RNAs, enhancer RNAs and repeats RNAs. YTHDC1 facilitates decay of a subset of these m^6A-modified RNAs, especially LINE1 elements, through the NEXT-mediated nuclear degradation. Reducing m^6A methylation by METTL3 depletion or site-specific m^6A demethylation of selected carRNAs elevates the levels of carRNAs and promotes open chromatin state and downstream transcription. Collectively, our results revealed that m^6A on carRNAs can globally tune chromatin state and transcription.

N^6-methyladenosine (m^6A) is an abundant modification on most eukaryote mRNAs (*1*, *2*), regulated mainly by "writer," "eraser," and "reader" proteins (*3*). The mRNA m^6A modification is installed by METTL3 (*4*), and can be removed by demethylases FTO and ALKBH5 (*5*, *6*). Readers, including the YTH domain family and HNRNP proteins, directly or indirectly recognize the m^6A-marked transcripts and affect mRNA metabolism (*4*, *7*–*9*).

m^6A plays critical roles in diverse biological processes, including the self-renewal and differentiation of embryonic and adult stem cells (*3*, *4*). In mouse embryonic stem cells (mESCs), transcripts encoding pluripotency factor tend to be m^6A methylated and subjected to YTHDF2-mediated decay in cytoplasm, which affects their turnover during differentiation (*10*–*12*). However, m^6A appears to also exhibit YTHDF2-independent regulations during early development, given that *Ythdf2* knockout mice can survive to late embryonic developmental stages, but *Mettl3* knockout results in early embryonic lethality (*11*, *13*). Interestingly, mouse knockout of the nuclear m^6A reader *Ythdc1* exhibits similar early mouse embryonic lethality to the *Mettl3* knockout (*14*). These observations imply that m^6A could play additional roles in nucleus that affect cell survival and differentiation. Previous studies also suggested that m^6A methylation on chromatin modifier transcripts or the chromosome binding of methyltransferase may impact transcription (*15*–*17*).

We thus investigated two independent *Mettl3* knockout (KO) mESC lines (*Mettl3*$^{-/-}$-1 and *Mettl3*$^{-/-}$-2) (*10*) and analyzed newly transcribed RNA levels. *Mettl3* KO mESCs displayed marked increases in nascent transcripts synthesis compared with control wild-type (WT) mESCs (Fig. 1A). We generated stable rescue cell lines that express WT METTL3 or an inactive mutant METTL3 (fig. S1A). The increased transcription of nascent transcripts upon *Mettl3* KO was reversed with WT but not mutant METTL3 (Fig. 1B).

We next asked if the global chromatin state is affected by *Mettl3* deletion. We performed DNase I-TUNEL assay and observed a notable increase in chromatin accessibility in *Mettl3* KO mESCs compared to WT. Moreover, expression of WT but not mutant METTL3 reversed the increased chromatin accessibility, suggesting m^6A dependence (Fig. 1, C and D).

We constructed conditional knockout (CKO) *Ythdc1* (fig. S1B) and *Ythdf2* (fig. S1C) mESCs. *Ythdc1* CKO showed a similar increase in transcription and chromatin openness as *Mettl3* KO (fig. S1, D and F), whereas *Ythdf2* CKO showed minimal differences (fig. S1, E and G). The changes observed

in *Ythdc1* CKO mESCs was reversed by expressing WT but not mutant YTHDC1 (fig. S1, B, D, and F). Consistently, both H3K4me3 and H3K27ac, two histone marks associated with active transcription, were elevated upon *Mettl3* and *Ythdc1* depletion (fig. S1, H and I). Together, these data suggested a nuclear regulatory role for RNA m^{6}A.

We next isolated non-ribosomal RNAs from soluble nucleoplasmic and chromosome-associated fractions and quantified m^{6}A/A by LC-MS/MS (fig. S2A). The m^{6}A/A ratio in non-ribosomal chromosome-associated RNAs (caRNAs) decreased the most (>50%) upon *Mettl3* KO (Fig. 2A and fig. S2B), suggesting an effect of m^{6}A on caRNAs. We immunoprecipitated ribosomal-RNA-depleted, m^{6}A-containing caRNAs and performed high-throughput sequencing (MeRIP-seq) in *Mettl3* KO and WT mESCs. The m^{6}A level showed a global decrease after *Mettl3* KO (fig. S2C), consistent with LC-MS/MS analysis (Fig. 2A). We identified ~40,000 peaks in each sample; both m^{6}A levels (fig. S2D) and peaks (fig. S2E) were fully reproducible. Compared to WT, *Mettl3* KO samples showed more hypomethylated peaks (fig. S2F), with the largest reduction found at intergenic regions (fig. S2, G and H).

We analyzed three types of caRNAs with potential regulatory functions: promoter-associated RNA (paRNA), enhancer RNA (eRNA) and RNA transcribed from transposable elements (repeats RNA), which we termed as chromosome-associated regulatory RNAs (carRNAs). The m^{6}A levels of these carRNAs were markedly decreased in *Mettl3* KO mESCs (Fig. 2B). Approximately 15-30% of all carRNAs contain m^{6}A in mESCs, with around 60% of which regulated by METTL3 (fig. S3A). These m^{6}A peaks contain GAC and AAC motifs, similar to those of the coding mRNAs (fig. S3, B and C). We categorized carRNAs into m^{6}A-marked and non-m^{6}A subgroups and found that the abundances of m^{6}A-marked transcripts, but not non-m^{6}A RNAs, were significantly elevated upon *Mettl3* KO (Fig. 2C and fig. S3D). Additionally, changes in m^{6}A levels negatively correlated with changes in expression levels for all three carRNA groups upon *Mettl3* KO (fig. S3E). Together, these data suggested that m^{6}A methylation destabilizes these carRNAs.

Previous work uncovered that YTHDC1 associates with components of the Nuclear Exosome Targeting (NEXT) complex, which is responsible for degradation of certain non-coding nuclear RNAs (*18*). We confirmed that YTHDC1 interacts with the NEXT components RBM7 and ZCCHC8 (fig. S4A). Because YTHDC1 is a known m^{6}A reader and *Ythdc1* CKO induced transcription up-regulation (fig. S1D), we hypothesized that YTHDC1 recognizes a subset of m^{6}A-marked carRNAs and triggers their decay through NEXT. Consistently, depletion of *Ythdc1* or *Zcchc8*, but not of *Ythdf2*, increased the m^{6}A/A ratio of caRNAs (fig. S4B). We subsequently performed MeRIP-seq of non-ribosomal caRNAs, and observed consistently increased m^{6}A level after *Ythdc1* depletion (fig. S4, C to E). We identified more hypermethylated peaks in *Ythdc1* CKO mESCs compared with controls (fig. S4F). The distribution of m^{6}A peaks on mRNA was not dramatically altered (fig. S4G), however, the proportion of m^{6}A peaks at intergenic regions increased upon *Ythdc1* CKO (fig. S4H). These suggested that YTHDC1, like METTL3, affects caRNAs transcribed mostly from intergenic regions.

We examined carRNAs and observed significantly increased m^{6}A for repeats RNAs upon YTHDC1 depletion (fig. S5A). Specifically, ~20-30% m^{6}A-marked paRNAs and eRNAs and more than 60% of m^{6}A-marked repeats RNAs are affected by YTHDC1 depletion, indicating a main role of YTHDC1 on affecting the stability of repeats RNAs in mESCs (fig. S5B). These m^{6}A peaks in different regions share similar motifs to those we detected previously (fig. S5, C and D). Moreover, we correlated m^{6}A fold-changes on three carRNA groups separately, and observed distinct negative correlations in all cases between *Mettl3* and *Ythdc1* depletion (fig. S5E), further indicating that YTHDC1 promotes decay of a portion of these carRNAs. We next performed nuclear RNA decay assays and observed notably increased half lifetime for all three groups of carRNAs upon *Ythdc1* CKO (Fig. 2D and fig. S5F). Moreover, the m^{6}A-marked RNAs from all three carRNA groups showed greater increases in half lifetime compared with non-m^{6}A RNAs after *Ythdc1* CKO (Fig. 2E and fig. S5G).

We then ranked repeats families according to their m^{6}A peak enrichment fold-changes in response to *Mettl3* or *Ythdc1* depletion, and identified the Long Interspersed Element-1 (LINE1) family as one of the most responsive in both cases (fig. S6, A and B). LINE1 elements are the most abundant class of mouse retrotransposon, transcribed in early embryos, and play critical roles in development, particularly remodeling chromatin structure and regulating transcription (*19*, *20*). We observed m^{6}A levels of each sub-family of LINE1 negatively correlate with their divergence: younger LINE1 contains higher m^{6}A level (fig. S6, C and D) and showed more significant methylation fold-changes (fig. S6, E and F) upon *Mettl3* or *Ythdc1* depletion. We next verified that the decay of L1Md_F, a representative young subfamily of LINE1, is regulated by YTHDC1 and METTL3 in an m^{6}A-dependent manner (supplementary text and figs. S6G and S7).

paRNAs, eRNAs and repeats RNAs such as LINEs can regulate transcription by affecting chromatin architecture at corresponding genomic loci. Because *Mettl3* KO increases both transcription and chromatin accessibility (Fig. 1), we next examined whether these changes are regulated by methylation of these carRNAs. We performed time-course RNA-seq of nascent transcripts as well as total nuclear RNAs, and conducted mammalian native elongating transcript sequencing (mNET-seq) (*21*, *22*) in *Mettl3* KO along with WT mESCs. Both the global expression level (Fig. 3, A and B) and transcription rate (Fig. 3, C and D, and fig. S8, A and B) increased

upon *Mettl3* KO. Indeed, genes that were up-regulated in *Mettl3* KO mESCs tend to have upstream carRNAs marked with m^{6}A more than down-regulated ones (Fig. 3, A and B). Moreover, genes with m^{6}A-marked upstream carRNAs attained higher increases in transcription rate than those with non-m^{6}A-marked upstream carRNAs, and the same is true when sorting genes with their pre-mRNAs not subjected to m^{6}A methylation (Fig. 3, E to F, and fig. S8, C to E), indicating that the reduced m^{6}A methylation of these carRNAs upon *Mettl3* KO activates the transcription of downstream genes.

Notably, we found all m^{6}A-dependent genes (~6,584) that showed reduced upstream carRNA methylation upon *Mettl3* depletion exhibited increased transcription rate (Fig. 3G). We further sorted those with transcription rate differences larger than 1 upon *Mettl3* KO (fig. S9A). They are mainly involved in transcription regulation, chromatin modification and stem cell population maintenance (fig. S9B). Hence, the reduced m^{6}A methylation of carRNAs not only promotes downstream transcription, but may activate genes involved in chromatin opening, initiating a positive feedback loop. We further analyzed *Prdm9, Kmt2d* (encoding two H3K4me3 methyltransferases), *Esrrb* and *Ranbp17* (related with differentiation), which all possess upstream carRNAs with reduced m^{6}A level upon *Mettl3* KO (fig. S10). Consistently, the half lifetime of these carRNAs and the transcription rate of their downstream genes both increased upon *Mettl3* KO, and these changes could be rescued by WT but not mutant METTL3 (fig. S11).

The interactions between super-enhancers and their target genes are known to be affected by transcription of exosome-regulated transcripts in mESCs (*23*). We thus examined super-enhancers and found that around 80% of super-enhancer RNAs (seRNAs) contain m^{6}A peaks (Fig. 3H and fig. S12A). The m^{6}A methylation level on seRNAs decreased (fig. S12, B and C) and the m^{6}A-marked seRNAs showed a greater increase in abundances compared to non-m^{6}A-marked ones upon *Mettl3* KO (Fig. 3I). seRNAs showing reduced m^{6}A upon *Mettl3* KO were associated with increased transcription rates at downstream genes (Fig. 3J); genes with transcription rate differences larger than one are mainly involved in transcription regulation, chromatin modification and stem cell maintenance (fig. S12, D and E), consistent with results obtained from other carRNAs (fig. S9). Moreover, we found that genes regulated by m^{6}A-marked upstream seRNAs tend to exhibit greater increases in transcription rate than those regulated by m^{6}A-marked upstream typical eRNAs upon *Mettl3* KO (fig. S12F).

We next turned to investigate chromatin state changes affected by altered carRNA methylation. We performed ChIP-seq and observed global increases of these two active marks, H3K4me3 and H3K27ac, upon *Mettl3* KO (fig. S13, A and B), consistent with the Western blot results (fig. S1H). Moreover, genes with m^{6}A-marked upstream carRNAs showed greater increases in H3K4me3 and H3K27ac than genes with non-m^{6}A upstream carRNAs in *Mettl3* KO mESCs (Fig. 4A). Likewise, *Mettl3* KO mESCs showed obvious increases in both marks at regions that flank METTL3-enriched DNA loci (fig. S13, C and D). These data suggested that stabilizing the upstream carRNAs in *Mettl3* KO mESCs could increase the deposition of active histone marks.

We suspect carRNAs could recruit proteins such as CBP/EP300 and YY1 to promote open chromatin and activate transcription (*24*, *25*). In fact, YY1 was identified as one of the top enriched transcription factors (TFs) at genomic regions that harbor m^{6}A-marked carRNAs (fig. S14A). Our ChIP-seq experiments indeed revealed global increases of EP300 and YY1 binding in *Mettl3* KO mESCs (Fig. 4, B and C), which correlating well with higher nearby eRNAs or paRNAs abundances (fig. S14, B and C). Moreover, both EP300 and YY1 binding negatively correlate with the m^{6}A level of nearby carRNAs (Fig. 4, D and E), and *Mettl3* KO leads to elevated EP300 and YY1 binding at regions that lose m^{6}A (Fig. 4, F and G). The genomic regions with both m^{6}A-marked carRNAs and binding of EP300 or YY1 showed the greatest increase in H3K27ac than regions with just m^{6}A or just EP300/YY1 binding upon *Mettl3* KO (Fig. 4H). We also performed ChIP-seq of JARID2, a component of the polycomb repressive complex 2 (PRC2), because RNA transcripts could repel PRC2 binding in order to maintain chromatin openness (*26*). We observed a globally decreased JARID2 binding, correlating well with the abundance increases of eRNAs and repeats transcripts upon *Mettl3* KO (fig. S14, D and E). Furthermore, JARID2 tends to bind to regions with high m^{6}A methylation of carRNAs (fig. S14F), with a positive correlation between the m^{6}A level on carRNA and local JARID2 binding changes upon *Mettl3* KO (fig. S14G). Therefore, these m^{6}A-regulated carRNAs may stabilize open chromatin state by not only recruiting active TFs but also repelling repressive factors such as PRC2 upon loss of methylation.

Lastly, elevated LINE1 may also modulate the global chromatin accessibility (*19*). We blocked LINE1 RNA in *Mettl3*$^{-/-}$ mESCs and observed overall reduced chromatin accessibility (Fig. 4I) (*20*). We employed fused CRISPR-dCas13b system (*27*) with either WT or inactive mutant FTO (fig. S15A). Only when targeting LINE1 by guide RNA (gRNA) with dCas13b-*wt* FTO but not dCas13b-*mu* FTO, we observed decreased m^{6}A level and increased half lifetime for LINE1, together with a globally increased chromatin accessibility (fig. S15, B to E). We then applied the dCas13b-FTO system to genes that harbor m^{6}A-marked upstream carRNAs (fig. S16). When targeting carRNAs using gRNAs and dCas13b-*wt* FTO, we observed site-specific methylation reduction, with little methylation changes observed using dCas13b-*mu* FTO or negative control gRNAs (Fig. 4J and fig. S17). We also observed increased half

lifetime of these carRNAs, up-regulation of downstream gene transcription and elevated local H3K4me3 and H3K27ac levels (Fig. 4J and fig. S18). Together, these results strongly support our discovery that m^{6}A methylation of carRNAs controls carRNA stability and downstream gene transcription.

To explore functional relevance of this m^{6}A-mediated regulation, we modulated LINE1 RNA level in WT and *Mettl3* KO mESCs. LINE1 abundance was elevated in *Mettl3* KO mESCs (fig. S19A) (*11*). Blocking LINE1 elevated differentiation capacity and decreased cell renewal in *Mettl3* KO mESCs (fig. S19, B to D). In contrast, targeting LINE1 by gRNA with dCas13b-*wt* FTO resulted in decreased differentiation capacity and increased cell renewal in WT mESCs but not with Cas13b-*mu* FTO (fig. S19, B to D). We also confirmed regulatory functions of m^{6}A-marked carRNAs in endometrial cancer progression, in which down-regulation of METTL3 increases cell proliferation, migration and tumor growth (supplementary text and figs. S20 to S23) (*28*).

Here, we report that carRNAs can be m^{6}A methylated by METTL3. A subset of these m^{6}A-marked carRNAs (mainly LINE1 repeats) are destabilized by YTHDC1 via the NEXT complex. We show that m^{6}A serves as a switch to affect abundances of these carRNAs, thus tuning nearby chromatin state and downstream transcription (Fig. 4K). The transcription activation induced by m^{6}A depletion is coupled with the increased chromatin accessibility, enrichment of certain TFs and active histone marks, revealing a direct crosstalk between carRNA m^{6}A methylation and chromatin state. Our findings demonstrate an additional layer of regulatory effect of carRNA m^{6}A on transcription.

REFERENCES AND NOTES

1. D. Dominissini, S. Moshitch-Moshkovitz, S. Schwartz, M. Salmon-Divon, L. Ungar, S. Osenberg, K. Cesarkas, J. Jacob-Hirsch, N. Amariglio, M. Kupiec, R. Sorek, G. Rechavi, Topology of the human and mouse m^{6}A RNA methylomes revealed by m^{6}A-seq. *Nature* **485**, 201–206 (2012). doi:10.1038/nature11112 Medline
2. K. D. Meyer, Y. Saletore, P. Zumbo, O. Elemento, C. E. Mason, S. R. Jaffrey, Comprehensive analysis of mRNA methylation reveals enrichment in 3′ UTRs and near stop codons. *Cell* **149**, 1635–1646 (2012). doi:10.1016/j.cell.2012.05.003 Medline
3. M. Frye, B. T. Harada, M. Behm, C. He, RNA modifications modulate gene expression during development. *Science* **361**, 1346–1349 (2018). doi:10.1126/science.aau1646 Medline
4. I. A. Roundtree, M. E. Evans, T. Pan, C. He, Dynamic RNA modifications in gene expression regulation. *Cell* **169**, 1187–1200 (2017). doi:10.1016/j.cell.2017.05.045 Medline
5. G. Jia, Y. Fu, X. Zhao, Q. Dai, G. Zheng, Y. Yang, C. Yi, T. Lindahl, T. Pan, Y.-G. Yang, C. He, *N*^{6}-methyladenosine in nuclear RNA is a major substrate of the obesity-associated FTO. *Nat. Chem. Biol.* **7**, 885–887 (2011). doi:10.1038/nchembio.687 Medline
6. G. Zheng, J. A. Dahl, Y. Niu, P. Fedorcsak, C.-M. Huang, C. J. Li, C. B. Vågbø, Y. Shi, W.-L. Wang, S.-H. Song, Z. Lu, R. P. G. Bosmans, Q. Dai, Y.-J. Hao, X. Yang, W.-M. Zhao, W.-M. Tong, X.-J. Wang, F. Bogdan, K. Furu, Y. Fu, G. Jia, X. Zhao, J. Liu, H. E. Krokan, A. Klungland, Y.-G. Yang, C. He, ALKBH5 is a mammalian RNA demethylase that impacts RNA metabolism and mouse fertility. *Mol. Cell* **49**, 18–29 (2013). doi:10.1016/j.molcel.2012.10.015 Medline
7. X. Wang, Z. Lu, A. Gomez, G. C. Hon, Y. Yue, D. Han, Y. Fu, M. Parisien, Q. Dai, G. Jia, B. Ren, T. Pan, C. He, *N*^{6}-methyladenosine-dependent regulation of messenger RNA stability. *Nature* **505**, 117–120 (2014). doi:10.1038/nature12730 Medline
8. X. Wang, B. S. Zhao, I. A. Roundtree, Z. Lu, D. Han, H. Ma, X. Weng, K. Chen, H. Shi, C. He, *N*^{6}-methyladenosine modulates messenger RNA translation efficiency. *Cell* **161**, 1388–1399 (2015). doi:10.1016/j.cell.2015.05.014 Medline
9. W. Xiao, S. Adhikari, U. Dahal, Y.-S. Chen, Y.-J. Hao, B.-F. Sun, H.-Y. Sun, A. Li, X.-L. Ping, W.-Y. Lai, X. Wang, H.-L. Ma, C.-M. Huang, Y. Yang, N. Huang, G.-B. Jiang, H.-L. Wang, Q. Zhou, X.-J. Wang, Y.-L. Zhao, Y.-G. Yang, Nuclear m^{6}A reader YTHDC1 regulates mRNA splicing. *Mol. Cell* **61**, 507–519 (2016). doi:10.1016/j.molcel.2016.01.012 Medline
10. P. J. Batista, B. Molinie, J. Wang, K. Qu, J. Zhang, L. Li, D. M. Bouley, E. Lujan, B. Haddad, K. Daneshvar, A. C. Carter, R. A. Flynn, C. Zhou, K.-S. Lim, P. Dedon, M. Wernig, A. C. Mullen, Y. Xing, C. C. Giallourakis, H. Y. Chang, m^{6}A RNA modification controls cell fate transition in mammalian embryonic stem cells. *Cell Stem Cell* **15**, 707–719 (2014). doi:10.1016/j.stem.2014.09.019 Medline
11. S. Geula, S. Moshitch-Moshkovitz, D. Dominissini, A. A. F. Mansour, N. Kol, M. Salmon-Divon, V. Hershkovitz, E. Peer, N. Mor, Y. S. Manor, M. S. Ben-Haim, E. Eyal, S. Yunger, Y. Pinto, D. A. Jaitin, S. Viukov, Y. Rais, V. Krupalnik, E. Chomsky, M. Zerbib, I. Maza, Y. Rechavi, R. Massarwa, S. Hanna, I. Amit, E. Y. Levanon, N. Amariglio, N. Stern-Ginossar, N. Novershtern, G. Rechavi, J. H. Hanna, m^{6}A mRNA methylation facilitates resolution of naïve pluripotency toward differentiation. *Science* **347**, 1002–1006 (2015). doi:10.1126/science.1261417 Medline
12. Y. Wang, Y. Li, J. I. Toth, M. D. Petroski, Z. Zhang, J. C. Zhao, *N*^{6}-methyladenosine modification destabilizes developmental regulators in embryonic stem cells. *Nat. Cell Biol.* **16**, 191–198 (2014). doi:10.1038/ncb2902 Medline
13. I. Ivanova, C. Much, M. Di Giacomo, C. Azzi, M. Morgan, P. N. Moreira, J. Monahan, C. Carrieri, A. J. Enright, D. O'Carroll, The RNA m^{6}A reader YTHDF2 is essential for the post-transcriptional regulation of the maternal transcriptome and oocyte competence. *Mol. Cell* **67**, 1059–1067.e4 (2017). doi:10.1016/j.molcel.2017.08.003 Medline
14. S. D. Kasowitz, J. Ma, S. J. Anderson, N. A. Leu, Y. Xu, B. D. Gregory, R. M. Schultz, P. J. Wang, Nuclear m^{6}A reader YTHDC1 regulates alternative polyadenylation and splicing during mouse oocyte development. *PLOS Genet.* **14**, e1007412 (2018). doi:10.1371/journal.pgen.1007412 Medline
15. Y. Wang, Y. Li, M. Yue, J. Wang, S. Kumar, R. J. Wechsler-Reya, Z. Zhang, Y. Ogawa, M. Kellis, G. Duester, J. C. Zhao, N^6-methyladenosine RNA modification regulates embryonic neural stem cell self-renewal through histone modifications. *Nat. Neurosci.* **21**, 195–206 (2018). doi:10.1038/s41593-017-0057-1 Medline
16. I. Barbieri, K. Tzelepis, L. Pandolfini, J. Shi, G. Millán-Zambrano, S. C. Robson, D. Aspris, V. Migliori, A. J. Bannister, N. Han, E. De Braekeleer, H. Ponstingl, A. Hendrick, C. R. Vakoc, G. S. Vassiliou, T. Kouzarides, Promoter-bound METTL3 maintains myeloid leukaemia by m^{6}A-dependent translation control. *Nature* **552**, 126–131 (2017). doi:10.1038/nature24678 Medline
17. B. Slobodin, R. Han, V. Calderone, J. A. F. O. Vrielink, F. Loayza-Puch, R. Elkon, R. Agami, Transcription impacts the efficiency of mRNA translation via co-transcriptional *N*^{6}-adenosine methylation. *Cell* **169**, 326–337.e12 (2017). doi:10.1016/j.cell.2017.03.031 Medline
18. M. Lubas, M. S. Christensen, M. S. Kristiansen, M. Domanski, L. G. Falkenby, S. Lykke-Andersen, J. S. Andersen, A. Dziembowski, T. H. Jensen, Interaction profiling identifies the human nuclear exosome targeting complex. *Mol. Cell* **43**, 624–637 (2011). doi:10.1016/j.molcel.2011.06.028 Medline
19. J. W. Jachowicz, X. Bing, J. Pontabry, A. Bošković, O. J. Rando, M.-E. Torres-Padilla, LINE-1 activation after fertilization regulates global chromatin accessibility in the early mouse embryo. *Nat. Genet.* **49**, 1502–1510 (2017). doi:10.1038/ng.3945 Medline
20. M. Percharde, C.-J. Lin, Y. Yin, J. Guan, G. A. Peixoto, A. Bulut-Karslioglu, S. Biechele, B. Huang, X. Shen, M. Ramalho-Santos, A LINE1-nucleolin partnership regulates early development and ESC identity. *Cell* **174**, 391–405.e19 (2018). doi:10.1016/j.cell.2018.05.043 Medline
21. A. Mayer, J. di Iulio, S. Maleri, U. Eser, J. Vierstra, A. Reynolds, R. Sandstrom, J. A. Stamatoyannopoulos, L. S. Churchman, Native elongating transcript sequencing reveals human transcriptional activity at nucleotide resolution. *Cell* **161**, 541–554 (2015). doi:10.1016/j.cell.2015.03.010 Medline
22. T. Nojima, T. Gomes, A. R. F. Grosso, H. Kimura, M. J. Dye, S. Dhir, M. Carmo-

Fonseca, N. J. Proudfoot, Mammalian NET-Seq reveals genome-wide nascent transcription coupled to RNA processing. *Cell* **161**, 526–540 (2015). doi:10.1016/j.cell.2015.03.027 Medline
23. E. Pefanis, J. Wang, G. Rothschild, J. Lim, D. Kazadi, J. Sun, A. Federation, J. Chao, O. Elliott, Z.-P. Liu, A. N. Economides, J. E. Bradner, R. Rabadan, U. Basu, RNA exosome-regulated long non-coding RNA transcription controls super-enhancer activity. *Cell* **161**, 774–789 (2015). doi:10.1016/j.cell.2015.04.034 Medline
24. D. A. Bose, G. Donahue, D. Reinberg, R. Shiekhattar, R. Bonasio, S. L. Berger, RNA binding to CBP stimulates histone acetylation and transcription. *Cell* **168**, 135–149.e22 (2017). doi:10.1016/j.cell.2016.12.020 Medline
25. A. A. Sigova, B. J. Abraham, X. Ji, B. Molinie, N. M. Hannett, Y. E. Guo, M. Jangi, C. C. Giallourakis, P. A. Sharp, R. A. Young, Transcription factor trapping by RNA in gene regulatory elements. *Science* **350**, 978–981 (2015). doi:10.1126/science.aad3346 Medline
26. X. Wang, R. D. Paucek, A. R. Gooding, Z. Z. Brown, E. J. Ge, T. W. Muir, T. R. Cech, Molecular analysis of PRC2 recruitment to DNA in chromatin and its inhibition by RNA. *Nat. Struct. Mol. Biol.* **24**, 1028–1038 (2017). doi:10.1038/nsmb.3487 Medline
27. S. Rauch, C. He, B. C. Dickinson, Targeted m^{6}A reader proteins to study epitranscriptomic regulation of single RNAs. *J. Am. Chem. Soc.* **140**, 11974–11981 (2018). doi:10.1021/jacs.8b05012 Medline
28. J. Liu, M. A. Eckert, B. T. Harada, S.-M. Liu, Z. Lu, K. Yu, S. M. Tienda, A. Chryplewicz, A. C. Zhu, Y. Yang, J.-T. Huang, S.-M. Chen, Z.-G. Xu, X.-H. Leng, X.-C. Yu, J. Cao, Z. Zhang, J. Liu, E. Lengyel, C. He, m^{6}A mRNA methylation regulates AKT activity to promote the proliferation and tumorigenicity of endometrial cancer. *Nat. Cell Biol.* **20**, 1074–1083 (2018). doi:10.1038/s41556-018-0174-4 Medline
29. J. Wuarin, U. Schibler, Physical isolation of nascent RNA chains transcribed by RNA polymerase II: Evidence for cotranscriptional splicing. *Mol. Cell. Biol.* **14**, 7219–7225 (1994). doi:10.1128/MCB.14.11.7219 Medline
30. A. M. Bolger, M. Lohse, B. Usadel, Trimmomatic: A flexible trimmer for Illumina sequence data. *Bioinformatics* **30**, 2114–2120 (2014). doi:10.1093/bioinformatics/btu170 Medline
31. D. Kim, B. Langmead, S. L. Salzberg, HISAT: A fast spliced aligner with low memory requirements. *Nat. Methods* **12**, 357–360 (2015). doi:10.1038/nmeth.3317 Medline
32. H. Li, B. Handsaker, A. Wysoker, T. Fennell, J. Ruan, N. Homer, G. Marth, G. Abecasis, R. Durbin, 1000 Genome Project Data Processing Subgroup, The Sequence Alignment/Map format and SAMtools. *Bioinformatics* **25**, 2078–2079 (2009). doi:10.1093/bioinformatics/btp352 Medline
33. Y. Zhang, T. Liu, C. A. Meyer, J. Eeckhoute, D. S. Johnson, B. E. Bernstein, C. Nusbaum, R. M. Myers, M. Brown, W. Li, X. S. Liu, Model-based analysis of ChIP-Seq (MACS). *Genome Biol.* **9**, R137 (2008). doi:10.1186/gb-2008-9-9-r137 Medline
34. A. R. Quinlan, I. M. Hall, BEDTools: A flexible suite of utilities for comparing genomic features. *Bioinformatics* **26**, 841–842 (2010). doi:10.1093/bioinformatics/btq033 Medline
35. S. Anders, P. T. Pyl, W. Huber, HTSeq—A Python framework to work with high-throughput sequencing data. *Bioinformatics* **31**, 166–169 (2015). doi:10.1093/bioinformatics/btu638 Medline
36. M. D. Robinson, D. J. McCarthy, G. K. Smyth, edgeR: A Bioconductor package for differential expression analysis of digital gene expression data. *Bioinformatics* **26**, 139–140 (2010). doi:10.1093/bioinformatics/btp616 Medline
37. H. Huang, H. Weng, W. Sun, X. Qin, H. Shi, H. Wu, B. S. Zhao, A. Mesquita, C. Liu, C. L. Yuan, Y.-C. Hu, S. Hüttelmaier, J. R. Skibbe, R. Su, X. Deng, L. Dong, M. Sun, C. Li, S. Nachtergaele, Y. Wang, C. Hu, K. Ferchen, K. D. Greis, X. Jiang, M. Wei, L. Qu, J.-L. Guan, C. He, J. Yang, J. Chen, Recognition of RNA N^6-methyladenosine by IGF2BP proteins enhances mRNA stability and translation. *Nat. Cell Biol.* **20**, 285–295 (2018). doi:10.1038/s41556-018-0045-z Medline
38. B. Langmead, C. Trapnell, M. Pop, S. L. Salzberg, Ultrafast and memory-efficient alignment of short DNA sequences to the human genome. *Genome Biol.* **10**, R25 (2009). doi:10.1186/gb-2009-10-3-r25 Medline
39. S. Heinz, C. Benner, N. Spann, E. Bertolino, Y. C. Lin, P. Laslo, J. X. Cheng, C. Murre, H. Singh, C. K. Glass, Simple combinations of lineage-determining transcription factors prime cis-regulatory elements required for macrophage and B cell identities. *Mol. Cell* **38**, 576–589 (2010). doi:10.1016/j.molcel.2010.05.004 Medline
40. W. A. Whyte, D. A. Orlando, D. Hnisz, B. J. Abraham, C. Y. Lin, M. H. Kagey, P. B. Rahl, T. I. Lee, R. A. Young, Master transcription factors and mediator establish super-enhancers at key cell identity genes. *Cell* **153**, 307–319 (2013). doi:10.1016/j.cell.2013.03.035 Medline
41. Y. Liao, G. K. Smyth, W. Shi, featureCounts: An efficient general purpose program for assigning sequence reads to genomic features. *Bioinformatics* **30**, 923–930 (2014). doi:10.1093/bioinformatics/btt656 Medline
42. R. Hubley, R. D. Finn, J. Clements, S. R. Eddy, T. A. Jones, W. Bao, A. F. A. Smit, T. J. Wheeler, The Dfam database of repetitive DNA families. *Nucleic Acids Res.* **44**, D81–D89 (2016). doi:10.1093/nar/gkv1272 Medline
43. D. W. Huang, B. T. Sherman, R. A. Lempicki, Systematic and integrative analysis of large gene lists using DAVID bioinformatics resources. *Nat. Protoc.* **4**, 44–57 (2009). doi:10.1038/nprot.2008.211 Medline
44. D. W. Huang, B. T. Sherman, R. A. Lempicki, Bioinformatics enrichment tools: Paths toward the comprehensive functional analysis of large gene lists. *Nucleic Acids Res.* **37**, 1–13 (2009). doi:10.1093/nar/gkn923 Medline

ACKNOWLEDGMENTS

We thank Dr. H. Chang for *Mettl3* knockout mESCs, Dr. J. Tauler and Dr. Angela Andersen from Life Science Editor for editing. **Funding:** This study was supported by the National Institute of Health HG008935 to C.H., Strategic Priority Research Program XDA16010506 to D.H., National Key R&D Program of China 2018YFA0109700 to D.H., National Institute of Health ES030546 to C.H., National Key R&D Program of China 2016YFA0100400 to Y.G. and Chuan C., China Scholarship Council (CSC) for the visit of Y.G. to the University of Chicago, Key research Program of Frontier Sciences, CAS (ZDBS-LY-SM013 to D.H.). The Mass Spectrometry Facility of the University of Chicago is funded by National Science Foundation (CHE-1048528). C.H. is an investigator of the Howard Hughes Medical Institute. **Author contributions:** C.H., J.L. and Y.G. conceived the original idea and designed original studies. J.L. performed most experiments with help from Y.G., Chuan C., C.L., and M.M.X. X.D. performed most computational analyses with initial discovery of carRNA methylation by Chuanyuan C., S.Z. and D.H. B.S. constructed most mESC lines. J.L., X.D. and C.H. wrote the manuscript with input from all authors. **Competing interests:** C.H. is a scientific founder and a member of the scientific advisory board of Accent Therapeutics, Inc. **Data and materials availability:** All sequencing data have been deposited in Gene Expression Omnibus (GSE133600 and GSE14561). All other data are available in the manuscript or the supplementary materials.

SUPPLEMENTARY MATERIALS

science.sciencemag.org/cgi/content/full/science.aay6018/DC1
Materials and Methods
Supplementary Text
Figs. S1 to S23
Tables S1 and S2
References (*29*–*44*)

2 July 2019; resubmitted 20 November 2019
Accepted 30 December 2019
Published online 16 January 2020
10.1126/science.aay6018

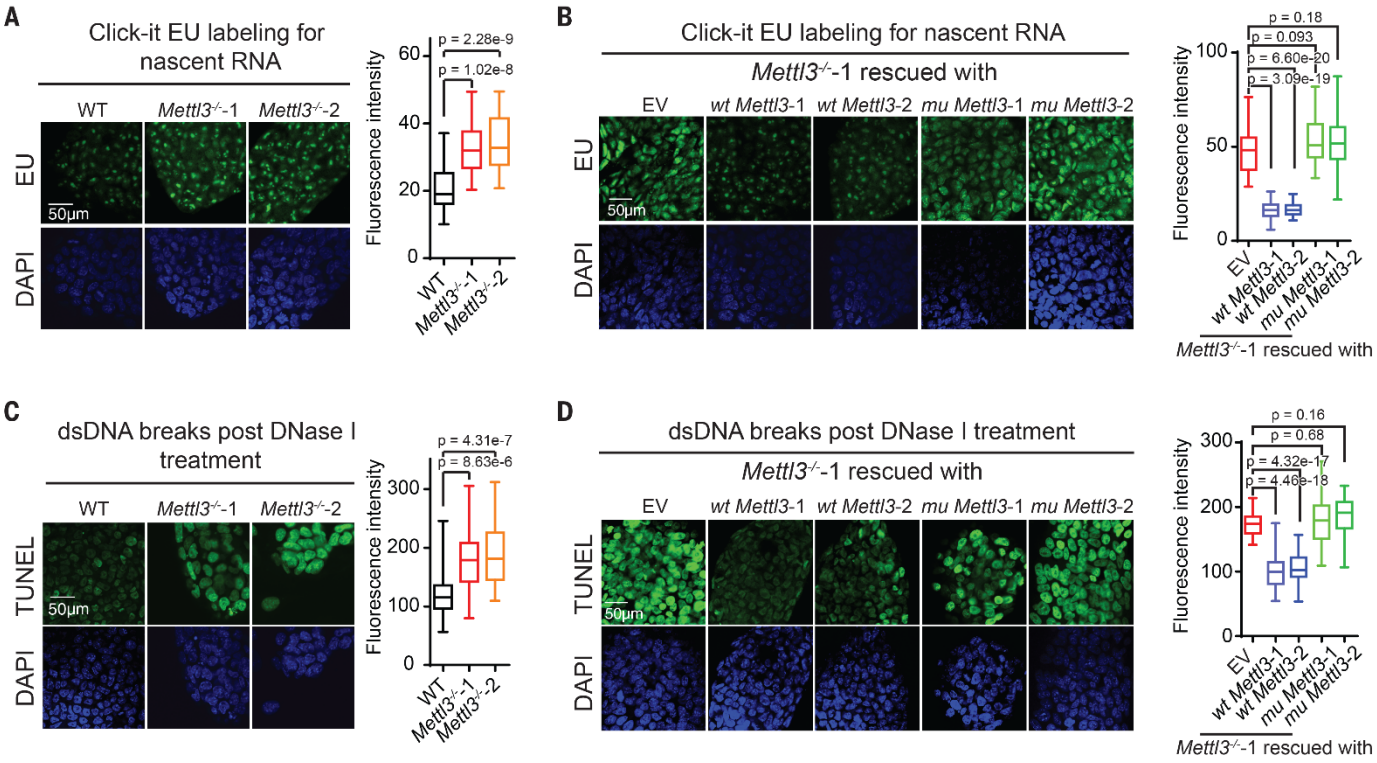

Fig. 1. *Mettl3* KO in mESCs leads to increased nascent RNA transcription and chromatin accessibility. (**A** and **B**) Analysis of nascent RNA synthesis in WT or *Mettl3*$^{-/-}$ mESCs (A, *Mettl3*$^{-/-}$-1 and -2 are two independently generated KO lines), and *Mettl3*$^{-/-}$ mESCs rescued with WT or an inactive mutant *Mettl3* (B). Nascent RNA synthesis was detected by using click-it RNA Alexa fluor 488 imaging kit. (**C** and **D**) Analysis of chromatin accessibility in WT or *Mettl3*$^{-/-}$ mESCs (C), and *Mettl3*$^{-/-}$ mESCs rescued with WT or mutant *Mettl3* (D). DNase I-treated TUNEL assay was performed. For panels A to D, nucleus is counterstained by DAPI. Scale, 50 μm. EV, empty vector, refers to *Mettl3*$^{-/-}$ mESCs when transfected with empty vector plasmid.

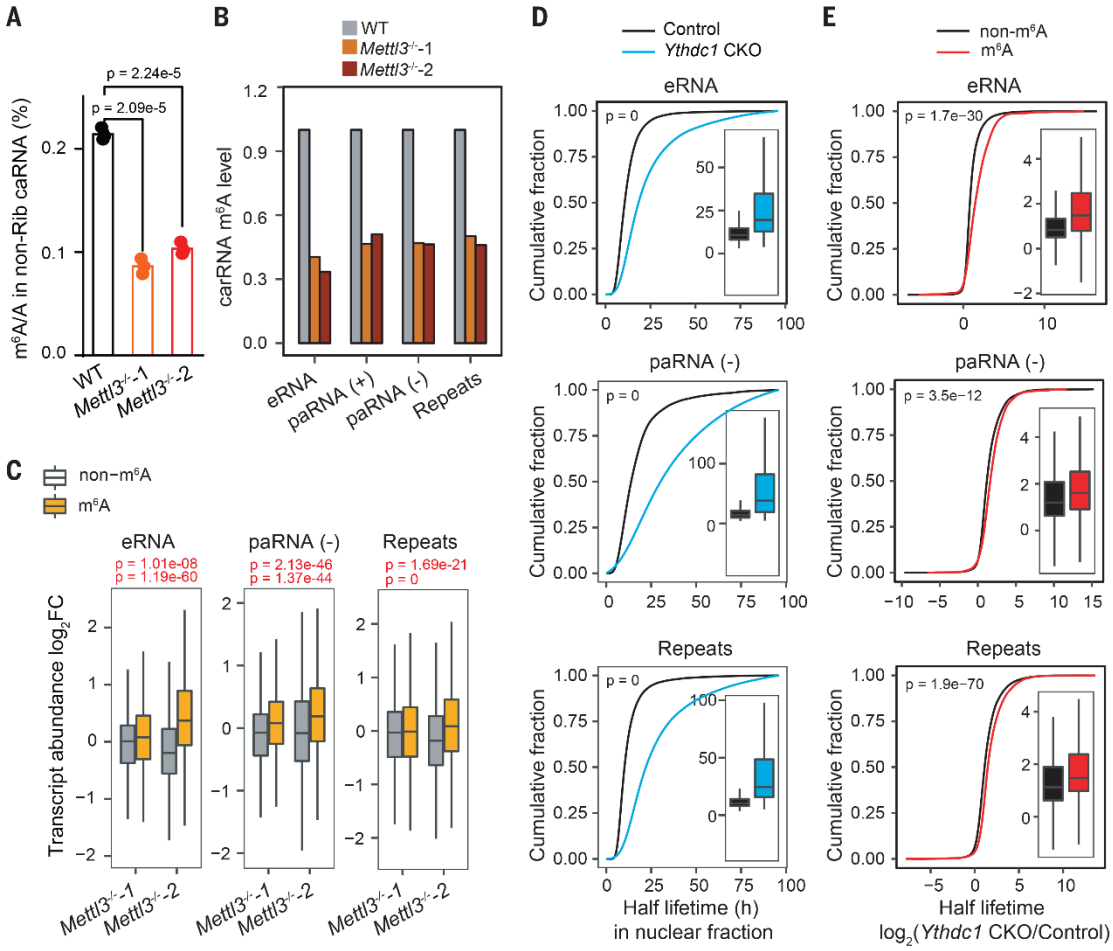

Fig. 2. Transcript turnover of carRNAs is regulated by m⁶A. (**A**) LC-MS/MS quantification of the m⁶A/A ratio in non-ribosomal caRNAs (including pre-mRNA) extracted from WT or *Mettl3*$^{-/-}$ mESCs, n = 3 biological replicates, error bars indicate mean ± s.e.m. (**B**) m⁶A level changes on carRNAs were quantified through normalizing m⁶A-seq results with spike-in between WT and *Mettl3* KO mESCs. n = 2 biological replicates. (**C**) carRNAs were divided into methylated (m⁶A) or non-methylated (non-m⁶A) groups. Boxplot showing greater increases in transcript abundance fold-changes of the m⁶A group versus non-m⁶A group upon *Mettl3* KO over WT mESCs. For panels A and C, p values were determined by two-tailed t-test. (**D**) Cumulative distribution and boxplots (inside) of nuclear carRNAs half lifetime changes in CKO *Ythdc1* and control mESCs. (**E**) Cumulative distributions and boxplots (inside) of the half lifetime changes of carRNAs upon *Ythdc1* CKO. carRNAs were divided into methylated (m⁶A) or non-methylated (non-m⁶A) groups. Depletion of YTHDC1 led to greater half lifetime increases of m⁶A-marked carRNAs than non-m⁶A-marked ones. For panels D and E, p values were calculated by a non-parametric Wilcoxon-Matt-Whitney test.

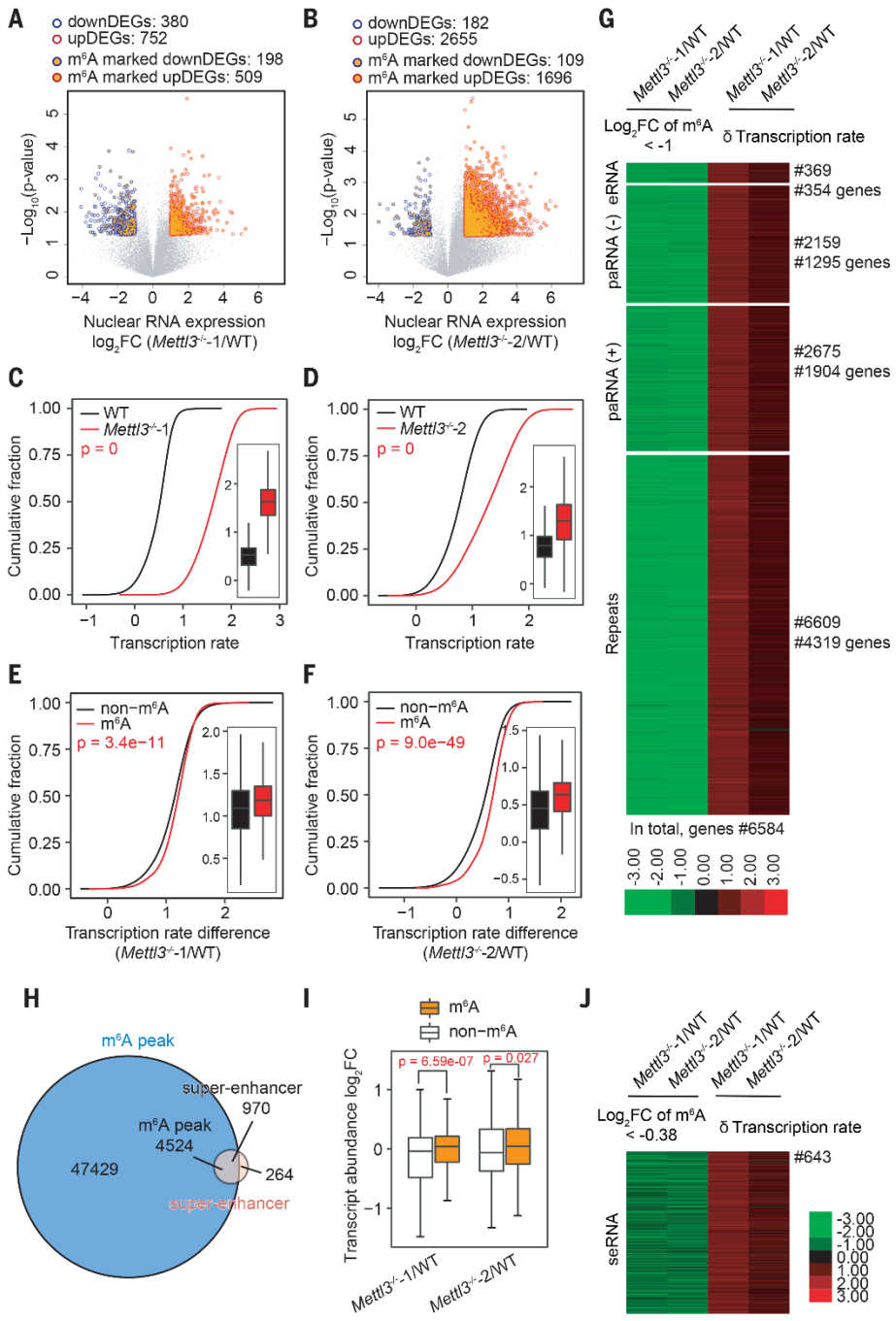

Fig. 3. The m^{6}A level of carRNAs affects downstream gene expression and transcription rate. (**A** and **B**) Volcano plot of genes with differential expression levels in *Mettl3*$^{-/-}$-1 (A) or *Mettl3*$^{-/-}$-2 (B) versus WT mESCs ($P < 0.05$ and $|\log_2FC| > 1$). Genes with upstream, m^{6}A-marked carRNAs were shown with orange circles. Gene expression level was normalized to ERCC spike-in with linear regression method. (**C** and **D**) Cumulative distribution and boxplot (inside) of gene transcription rate in *Mettl3*$^{-/-}$-1 (C) or *Mettl3*$^{-/-}$-2 (D) versus WT mESCs. (**E** and **F**) Cumulative distribution and boxplot (inside) of transcription rate difference between *Mettl3*$^{-/-}$-1 (E) or *Mettl3*$^{-/-}$-2 (F) versus WT mESCs. Genes were categorized into two subgroups according to whether their upstream carRNAs contain m^{6}A (m^{6}A) or not (non-m^{6}A). For panels C to F, *p* values were calculated by a non-parametric Wilcoxon-Matt-Whitney test. (**G**) Heatmap showing the m^{6}A level fold-changes ($\log_2FC < -1$) on carRNAs and downstream gene transcription rate difference between *Mettl3* KO and WT mESCs. (**H**) Venn diagram showing the overlap between the m^{6}A peaks and super-enhancer peaks in mESCs. (**I**) Boxplot showing fold changes of the abundance of m^{6}A-marked and non-m^{6}A-marked seRNAs between *Mettl3*$^{-/-}$ and WT mESCs. For panels A, B and I, *p* values were determined by two-tailed *t*-test. (**J**) Heatmap showing fold-change ($\log_2FC < -0.38$) of m^{6}A level of seRNAs and transcription rate difference of their downstream genes between *Mettl3* KO and WT mESCs.

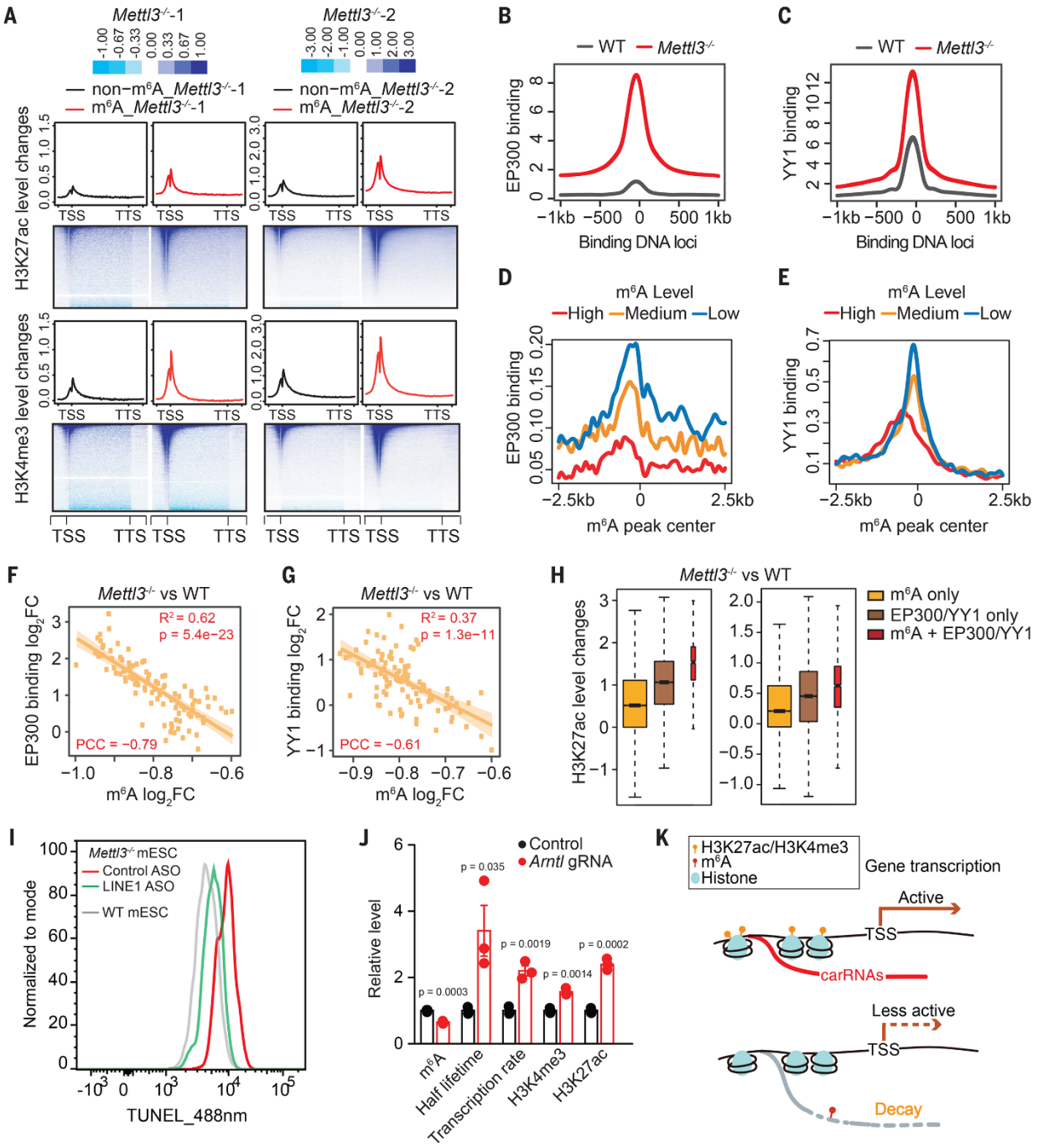

Fig. 4. The m^{6}A level of carRNAs affects local chromatin state and downstream transcription. (**A**) Profiles of H3K27ac (top panel) and H3K4me3 (bottom panel) level changes on gene body together with 2.5 kb upstream of TSS and 2.5 kb downstream of TTS in WT and *Mettl3* KO mESCs. Genes were categorized into two groups according to whether they harbor upstream m^{6}A-marked carRNAs (m^{6}A) or not (non-m^{6}A). (**B** and **C**) Profiles of EP300 (B) or YY1 (C) DNA binding at their peak center and flanking 2.5 kb regions in WT and *Mettl3* KO mESCs. (**D** and **E**) Profiles of EP300 (D) and YY1 (E) DNA binding at the center of m^{6}A peaks overlapped with carRNAs and its flanking 2.5 kb regions in WT mESCs. m^{6}A peaks were categorized into highly (High), moderately (Medium) or lowly (Low) methylated groups according to their m^{6}A levels in WT mESCs. (**F** and **G**) The correlation between changes in m^{6}A level of the carRNAs and changes in EP300 (F) or YY1 (G) DNA binding at genomic regions that show m^{6}A differences with *Mettl3* KO. The genomic regions were categorized into 100 bins based on fold change rank of m^{6}A level upon *Mettl3* KO. (**H**) Barplots showing H3K27ac level changes at genomic regions that are m^{6}A methylated (m^{6}A only, without EP300 and YY1 binding), bound by EP300 or YY1 (EP300/YY1 only without m^{6}A carRNA), and m^{6}A methylated with EP300 and YY1 binding (m^{6}A + EP300/YY1). The last group showed the highest increase upon *Mettl3* KO. (**I**) Analysis of chromatin accessibility in *Mettl3* KO mESCs treated with control or LINE1 antisense oligos (ASOs). DNase I-treated TUNEL assay was performed. (**J**) A dCas13b-FTO (WT or inactive mutant) construct with guide RNA (gRNA) targeting the seRNA of *Arntl* was used to reduce the m^{6}A level of *Arntl* seRNA. After treatment, increased half lifetime of the target seRNA, elevated local H3K27ac and H3K4me3 levels, and increased *Arntl* transcription rate were observed, accompanied with the decreased seRNA m^{6}A level. (**K**) A schematic model showing how m^{6}A affects transcription by regulating the decay of upstream carRNAs stability and chromatin state.

N^6-methyladenosine of chromosome-associated regulatory RNA regulates chromatin state and transcription

Jun Liu, Xiaoyang Dou, Chuanyuan Chen, Chuan Chen, Chang Liu, Meng Michelle Xu, Siqi Zhao, Bin Shen, Yawei Gao, Dali Han and Chuan He

published online January 16, 2020